MicaSense Aerial Pointing and Stabilization System: Dampening In-Flight Vibrations for Improved Agricultural Imaging

Zachary Caratao [*], Kelsey Gabel[*], Abijit Arun[*], Brett Myers,[*]

Autonomous Flight Systems Laboratory, University of Washington, Seattle, WA, 98195, USA

David Swartzendruber,[†]

MicaSense, Inc., Seattle, WA, 98103, USA

Christopher W. Lum[‡]

Autonomous Flight Systems Laboratory, University of Washington, Seattle, WA, 98195, USA

This paper describes the design, manufacturing, testing, and evaluation of an unmanned aerial system (UAS) gimbal designed to stabilize multiple sensors. The gimbal is designed to carry the MicaSense RedEdge multispectral camera as well as the FLIR Vue Pro R infrared camera which are used in precision agriculture applications. The gimbal is designed to be modular in the sense that the gimbal can interface with a wide range of aircraft. Trade studies and design compromises related to the design of the gimbal are presented. The gimbal is designed to balance functionality with manufacturability and economic viability. In addition to detailing the engineering design of the gimbal, this paper outlines the testing campaign to validate the functionality of the gimbal. Various metrics are used to assess and evaluate the performance of the system. These metrics are targeted to the specific application of precision agriculture with UAS.

Nomenclature

AFSL	Autonomous Flight Systems Laboratory
AGL	Above Ground Level
GCS	Ground Control System
CG	Center of Gravity
FVPR	FLIR Vue Pro R
IMU	Inertial Measurement Unit
IR	Infrared
MAPSS	MicaSense Aerial Pointing and Stabilization System
MTF	Modulation Transfer Function
NDVI	Normalized Difference Vegetation Index
COTS	Commercial Off-The-Shelf
PIC	Pilot in Command
PID	Proportional Integrator Differentiator
UA/UAS/UAV	Unmanned Aircraft/Unmanned Aerial System/Unmanned Aerial Vehicle
UW	University of Washington

[*]Undergraduate, Department of Aeronautics and Astronautics, Seattle, WA 98195, AIAA Student Member.
[†]Lead Mechanical Engineer, MicaSense, Inc., Seattle, WA, 98103
[‡]Research Assistant Professor, Department of Aeronautics and Astronautics, Seattle, WA 98195, Member AIAA.

American Institute of Aeronautics and Astronautics

I.   Introduction

By far the most popular payload carried by modern unmanned aircraft systems (UAS) is a camera. Cameras have been applied to problems such as search and rescue,[1] wildfire detection,[2] and formation flight.[3] More recently, applications such as mapping and precision agriculture[4] have become popular. Continuing this development, the University of Washington's (UW) Aerospace and Aeronautics (UWAA) Senior Capstone Program and MicaSense, Inc. have collaborated to develop UAS technology relevant to precision agriculture. Similar to other UWAA Senior Capstone Programs,[5,6] a team of undergraduates collaborate with an industry sponsor to complete an intensive project addressing current engineering challenges. Through the Senior Capstone Program and MicaSense, a standalone UAS gimbal capable of carrying two different optical sensors was developed.

MicaSense, Inc.[7] is a remote sensing and analytics company that provides data-based solutions for agriculture. Through advanced sensing hardware and data processing software, their aim is to bring precision monitoring and diagnostics to the agricultural industry. The MicaSense RedEdge multispectral camera was designed to provide crop growers the ability to survey their crops through five different wavebands: blue, green, red, red edge, and near IR. Synthesizing these five viewing bands into false-color images allows farmers to observe the rigor of their crop, fertilizer coverage and track variations over time.[8] Within this project, the goal is to create a gimbal that houses both the RedEdge and a separate camera: the FLIR Vue Pro R. The two sensors can be seen in Fig. 1. The FLIR Vue Pro R (FVPR) is a thermal imaging camera designed by FLIR Systems, Inc. By pairing the two cameras, MicaSense hopes to provide its customers with a wider range of sensing functionality. The problem addressed in this study is to design one structurally sound gimbal for two separate camera payloads that simultaneously mitigates vibrations while keeping both sensors pointed nadir at all times during flight. The cameras must also maintain rigid to each other, keeping their optical axes aligned during the entire duration of the flight.

Fig. 1. The two sensors that will be attached to the gimbal system. On the left is the MicaSense RedEdge[9]and on the right is the FLIR Vue Pro R.[10] The dimensions include the length, height, and width (including protruding lens).

Using their advanced sensors, MicaSense provides their customers with maps such as normalized difference vegetation indices[11] (NDVI, Fig. 2), digital elevation models[4] (DEM), and others. These maps allow farmers to quickly and easily perform diagnostics on their vegetation. Without these tools, farmers are prone to preventable losses such as improper irrigation or disease. The problem is that many customers struggle to achieve the necessary amount of photo overlap to create useful and accurate crop health maps. Most customers will opt for a fixed support/attachment for their RedEdge camera. With such a support the sensor will not point toward the ground at all times making a gimbal a necessary addition to the system.

American Institute of Aeronautics and Astronautics
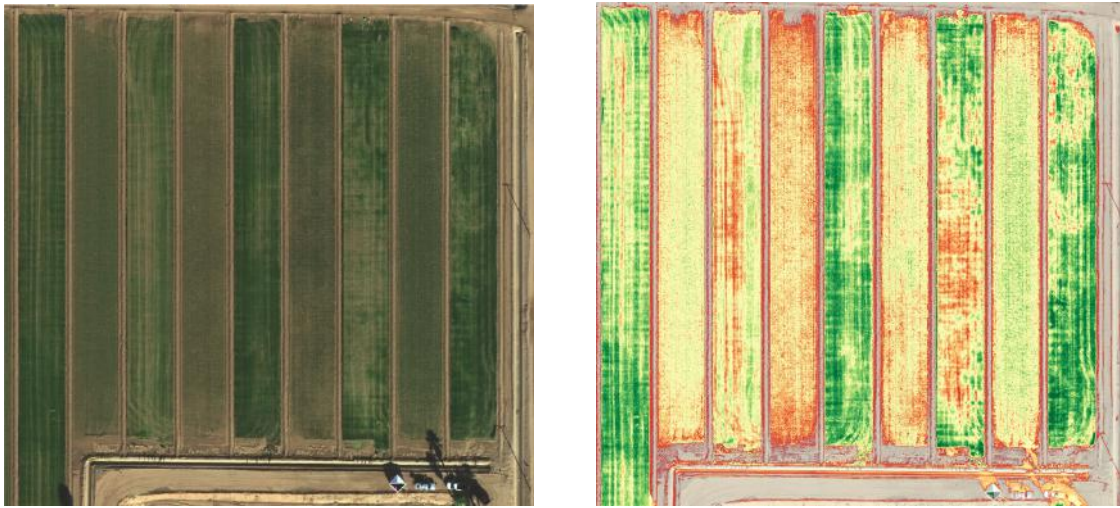
Fig. 2. A RGB map on the left and its resulting normalized difference vegetation index (NDVI) map on the right. These maps were produced by MicaSense's proprietary Atlas software as a sample dataset. The NDVI map helps farmers to analyze crop health. The slightly darker areas indicate higher crop strain.[12]

A gimbal is a pivoted support that reacts to and filters rotation about one or more axes. Gimbals are commonly used to support cameras because they stabilize and dampen out vibrations effectively. Both vibration dampening and accurate aerial pointing are needed for a camera to take quality pictures. The problem, however, is that most commercially available gimbals are fitted to serve a few different commonly used, types of cameras (DSLR, GoPro, etc.) and almost no readily available gimbal fits multiple camera payloads. Engineers at MicaSense Inc. have spent a significant amount of time trying to provide customers with recommendations for off-the-shelf multicopter gimbals with limited success. This paper describes a development of a solution to this problem in the form of a multi-camera, modular UAS gimbal, hereafter referred to as the MicaSense Aerial Pointing and Stabilization System (MAPSS).

II.   Model

Developing MAPSS from concept to production relies on various engineering decisions on the electronics that power the RedEdge and FVPR and move the gimbal to mechanical designs that house the camera payloads.

A.   Electronics

The main electrical components for MAPSS are shown in Fig. 3 and include the gimbal controller, brushless gimbal motors, and the Matek Mini Power Hub. The MAPSS electrical system utilizes off-the-shelf components and is designed to power all components of MAPSS directly from the UAS main power battery supply via an XT60 connection. The Martinez gimbal controller was chosen for its economic cost and 2 Axis control support. Brushless gimbal motors were chosen for their superior small angular rotations compared to servos. Specifically the Turnigy HD 3506 Brushless Gimbal Motors, were chosen for their lower weight (109g per motor) and sufficient torque to carry a payload of 400g.
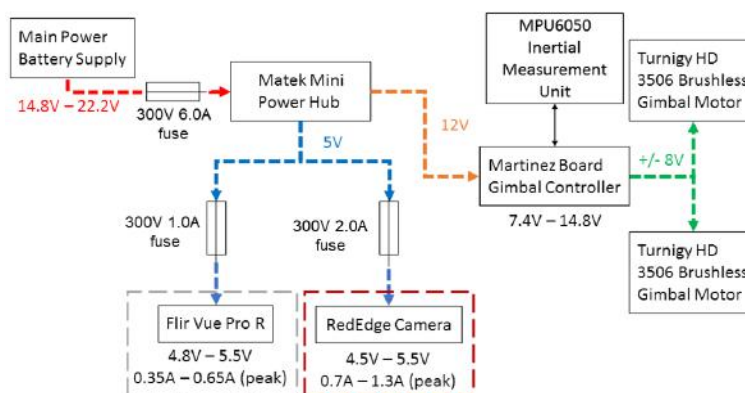
American Institute of Aeronautics and Astronautics

Fig. 3. Electrical system diagram outlining voltages and requirements of the desired components.

As a standalone product, the gimbal must be solely powered from the main power supply of the aircraft to cut down on payload weight requirements and ease integration. UAS designed to carry both cameras and perform these type of missions typically used 4S to 6S batteries (14.8V to 22.2V) as a main power supply. Various precautions were considered to mitigate current fluctuations caused by propeller motors, adapt to different UAS batteries, and remain within the power requirements of the electrical components. As shown in Fig. 3, the Matek Mini Power Hub was chosen to step down the main power supply into 5V for powering the cameras and 12V for powering the Martinez gimbal controller. The Matek uses DC/DC buck regulators with a 95% efficiency to step down the voltage without causing excessive heat compared to linear regulators.[13]

For safety, the electrical system also contains in-line fuses in case of any short circuits that could damage MAPSS cameras or other UAV systems. In-line fuses were chosen for economic cost and customer ease of use and replaceability. While the pilot is responsible for avoiding dangerous high-current draw situations, these fuses act as a backup to prevent damage to expensive camera equipment.

B. Mechanical Design

The gimbal design optimized for low weight and utilizes a fixture plate for housing the two camera systems. As can be seen in Fig. 4, both cameras are fixed on the plate and point in one direction. The mounting scheme for the FVPR is completely different than that of the RedEdge. The FVPR is normally fastened with hardpoints on the sides while the RedEdge is secured on the back of the camera.[14] This creates difficulties when designing a plate for both sensors to attach to. To address this, the FVPR is fastened to the fixture plate using an additional plate and binding posts while the RedEdge is screwed in through the back. By fastening the FVPR and RedEdge in this manner, the optical axes of both cameras remain aligned during flight. Accurate alignment was critical in this application as any misalignment introduces inconsistency in image quality and analysis between both cameras.

By designing with weight optimization as a high priority, MAPSS would be viable on multiple aircraft with different payload requirements and require less power from the UAS to point MAPSS nadir. With a lighter payload, lower torque gimbal motors which use less power from the UAS Main Power Battery Supply can be utilized. Many design revisions were considered for this purpose, from 3D printed ABS to the final decision of utilizing low weight sheet aluminum as seen in Fig. 8 and various camera housing options from mounting options on both cameras to finalizing designs on a separate external plate.
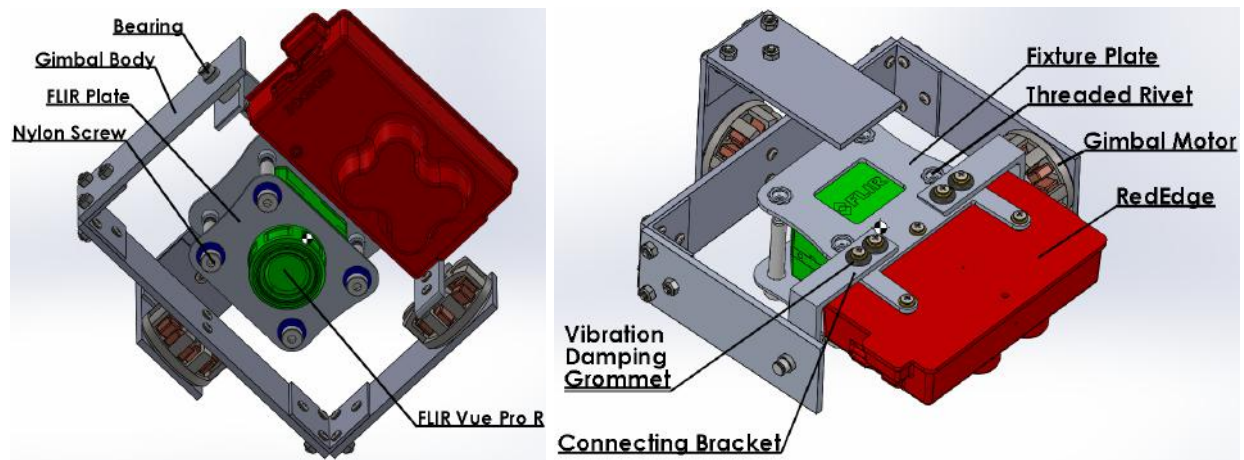
American Institute of Aeronautics and Astronautics

Fig. 4. Rendering of MAPSS with CG and labels. The white icon near the center indicates the CG for the system.

Another major design consideration is the center of gravity. By aligning the CG with the gimbal motors, the amount of torque and power needed to make precise angular rotations is reduced. This reduction in power drawn from the multirotor battery allows for longer flight durations. CG alignment also keeps the resting position of the gimbal flat and facing nadir. SolidWorks was used to model the CG of the system. A virtual 3D model of the RedEdge was provided by MicaSense and a virtual 3D model of the FVPR was taken from the FLIR website. A model of MAPSS taken from SolidWorks in Fig. 4 shows the CG of the system in relation to the other components. The RedEdge is approximately 50g heavier than the FVPR on its own, so the CG of the system is closer to the RedEdge than the FVPR.

Table 1. Assembled mass breakdown of final gimbal configuration.

Item	Mass (g)	Comments
Turnigy Gimbal Motor 3506	68	Tilt motor including connectors and wires
Turnigy Gimbal Motor 3506	68	Roll motor including connectors and wires
Fixture Plate	62	Includes IMU, cords and screws
FLIR Plate	20	Includes nylon screws and washers
L Bracket	87	Includes screws, nuts, and connecting bracket
Bearing	11	With bushing and retaining washer
C Bracket	303	Includes screws, nuts, and connecting brackets
Total MAPSS Gimbal	**619**	Gimbal only, no payload

To keep the RedEdge and the FVPR capturing the same field of view, the sensors had to match orientations on the fixture plate. Affixing the FVPR to the fixture plate while keeping the same orientation as the RedEdge proved to be difficult using the native mounting hardware. Instead of using the native mounting points, a sandwiching method was used to attach the FVPR. This method used a smaller plate, referred herein as the FLIR plate, which had 4 screws that sandwiched the FVPR between the fixture plate and the FLIR plate. This method of attachment prevented any rattling of the FVPR and required less precise tolerances for manufacturing. A 3D model of this attachment is shown in Fig. 6.

American Institute of Aeronautics and Astronautics
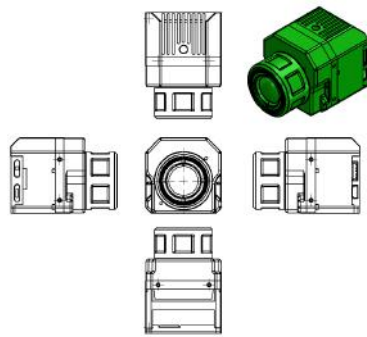
Fig. 5. The smaller FVPR screw points are on the left, right and bottom faces. The large screw point is on the top face.
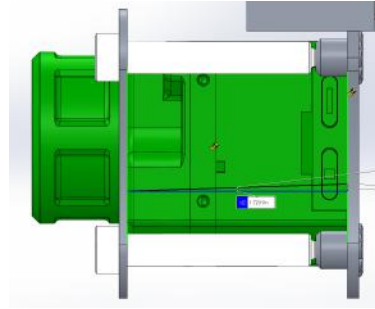
Fig. 6. The attachment mechanism for adhering the FVPR to the fixture plate.

Vibration damping is another important design criteria. The RedEdge takes every one of its five images on a global shutter[8] where every pixel is captured simultaneously. This prevents the images from the RedEdge from being overly effected by the motion of the aircraft. The FVPR takes images with a rolling shutter in the form of video with pixels captured within a period of 12ms.[14] Under unstable circumstances, this delay has the potential to generate skewed and blurry images as seen in Fig. 7.
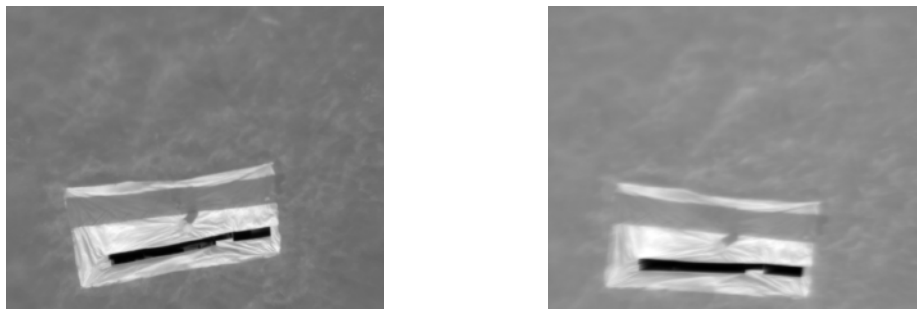
Fig. 7. Comparison of FVPR images. The left image has been stabilized with MAPSS operational while the right image blurred without MAPSS .

In order to account for the FVPR's rolling shutter, several vibration dampening components were included within MAPSS. The largest damping piece on the gimbal is the damping plate shown in Fig. 8. This plate interfaces between the UAV mount and the rest of the gimbal and contains 100g isolation rated vibration dampening balls. These rubber balls are found on most drone and gimbal websites and are used in various parts of the drone in various sizes and stiffness. They are inserted holes into two plates, one which is bolted to the UAV and a lower plate which is connected to the body of the gimbal, such that the gimbal hangs with no hard connection the UAV. The main trade-off in varying these is that a stiffer connection allows more vibrations to travel through to the payload of the gimbal, but a softer connection can allow the gimbal to swing under its own weight and due to wind gusts. Along with the damping plate, vibration damping grommets were part of the connecting brackets as seen in Fig. 4 and Fig. 8. These stopped vibrations that originated within the gimbal system, such as vibrations from gimbal motors, wind induced vibrations and other unforeseen source of vibration. Vibration dampening pieces were not placed within the fixture plate system to preserve camera alignment during vibrations.

American Institute of Aeronautics and Astronautics

Fig. 8. Final MAPSS setup showcasing the final product utilized in this paper. The left image displays the dampening plate and structure without the Fixture Plate, FLIR Plate, and sensors installed. The center image shows MAPSS with the RedEdge and a 3D printed model of the FVPR installed. The right image shows MAPSS fully operational and mounted on the UAV used for testing on the right.

Since this work was being done for a company that had small scale production in mind, several of the described structural aspects were chosen due to a desire to minimize cost, reduce labor time for fabrication and assembly, and reduce the number of custom pieces needed. The prototype is made primarily out of aluminum 6061-T6 plates and bars, since they are common, low cost, high strength materials that are easy to machine. The gimbal arms are all made out of the same width bar to reduce material costs and waste. The connecting brackets are uniform and the camera plate and dampening plate are also the same thickness to allow for efficient cutting via water jet. Total labor time for fabrication of the custom pieces is less than 1 hr per unit for an efficient machine shop and assembly of the gimbal is 0.5 hr, neglecting mounting the cameras and attaching the gimbal to the UAV.

Several structural enhancements were examined for future developments such as using round tubing in place of flat sheets and carbon fiber in place of aluminum. Round tubing would have been better for several of the arm pieces due to the increased stiffness in torsion, but connecting these would require either welding or special connectors. Since the strongest aluminum alloys are typically tempered, they often cannot be welded or they require tempering after the welding is complete. Easily weldable alloys typically have less than half the strength of tempered aluminum. The tubing connectors are bulky and expensive, or they would need to be custom made, which adds significant cost. Choosing the most efficient and structurally sound design with a custom carbon fiber layup would quickly increase production costs and required extensive, complex finite element analysis. As a result, it was determined to be too costly to design and produce in large quantities.

However, the current design can have nearly all of the structural components replaced with pre-made carbon fiber sheets cut with a waterjet. This would reduce manufacturing time and weight, while increasing cost. The downside of using pre-made sheets is that convenient suppliers often give little information about the specific type of composite used and ply orientation. This makes structural analysis and weight optimization difficult, but it would likely still be worth the trade off for the production model. The density of a carbon fiber plate is 1.661 g/cm^3 compared to 2.712 g/cm^3 for aluminum so switching all of the aluminum bars and plates to carbon fiber with a thickness of 0.25cm would give a weight savings of 110g.

C. Structural Analysis

The gimbal plate structure was modeled in a finite element software package to check the deformation of the fixture plate under the compressive threading loads from the cameras. To simulate loading, a distributed load of 18.35N was placed over the RedEdge mounting points to simulate the average torque loading of a steel 4-40 thread screw (0.621Nm).[15] While a distributed load of 5.43N was placed over the FVPR mounting points to simulate the maximum torque before deformation of a nylon 10-24 thread screw (0.452Nm).[16]

Fig. 9 shows the final results of the analysis using Dassault Systemes' finite element program Abaqus. Even with a safety factor of 2, the maximum deflection was on the magnitude of .003cm, a value that will not offset the optical axis enough to affect the results.

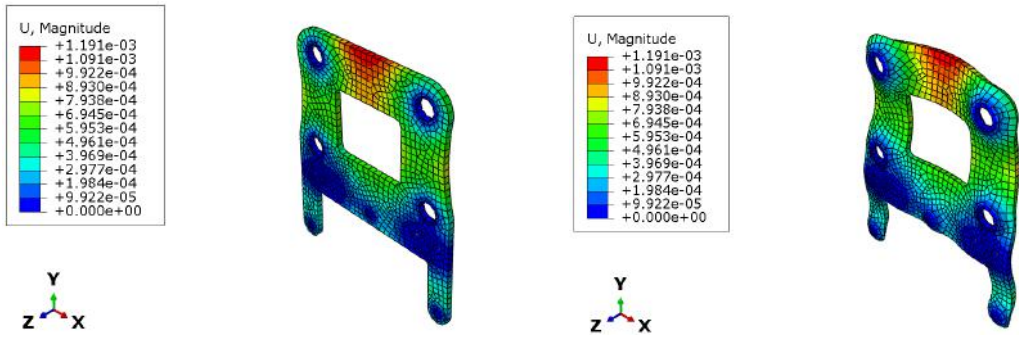American Institute of Aeronautics and Astronautics

Fig. 9. FEA showing deformation of the fixture plate under loading. The left image shows the accurate picture while the right has the deformations exaggerated 300 times larger.

III.   Experimental Methods

In order to verify the effectiveness of MAPSS to mitigate in-flight vibration and continuously point the camera payload nadir, MAPSS was flight tested in comparison with an commercial, off-the-shelf (COTS) gimbal as seen in Fig. 10. This COTS gimbal is made from an LD Storm Eye Brushless Gimbal Full Carbon Kit[17] outfitted with the same electronic system as MAPSS. Data gathered in-flight includes vibration data from a vibration sensor consisting of an Arduino Uno, a GY-521 breakout board, and a MPU6050 chip.[18,19] attached to the camera payload plate and footage from the RedEdge and FVPR. Specific images from the footage would be analyzed through image resolution analysis known as modulation transfer functions (MTF). By comparing the vibration data and image quality between the gimbals, the increase in image quality experienced by using MAPSS can be quantified.

A.   Flight Test Procedure

A standardized flight test procedure was used to expose the gimbal to in-flight vibrations. A DJI S1000+ was chosen as the testing platform for its stability and its ability to carry a larger selection of gimbal configurations due to its carrying capacity (4kg) and available space (305x305x152mm) under the multicopter.[20]

Following the Federal Aviation Administration (FAA) Small UAS Rule (14 CFR part 107),[21] the flight testing was operated in Class G airspace away from pedestrians and under direct supervision by a remote pilot certificate holder. Much of the infrastructure to support flight testing was provided by the UW AFSL.[22,23]

The flight test procedure was to attach a gimbal configuration onto the S1000+, activate recording functions in the RedEdge and FVPR and hover the S1000+ 15.24m AGL over a test image/article to generate data for later MTF analysis. 15.24m represents the lowest altitude recommended for conducting aerial surveys. This lower altitude also allows for easier visual observation of the gimbal in flight as well as reducing the size of the MTF test article.

To emulate customer configurations for attaching cameras such as the RedEdge and FVPR for in-flight surveying purposes, three different configurations were chosen as shown in Table 2.

**Table 2. Different gimbal conditions used for testing.**

Gimbal Configuration	Gimbal On	Gimbal Locked	Gimbal Locked and Dampening Plate Removed
Conditions	Martinez Board Active	Martinez Board Inactive	Martinez Board Inactive
	Motors Free to Move	Motors Locked	Motors Locked
	Dampening Plate Installed	Dampening Plate Installed	Dampening Plate Removed

The first configuration, "Gimbal On", has the gimbal stabilizing with the vibration dampening plate interfacing between the gimbal and UAV. This configuration was expected to be the optimal test configuration due to its vibration dampening and nadir stabilization. The second configuration, "Gimbal Locked", locks

American Institute of Aeronautics and Astronautics

the motors of the gimbal in place, preventing active stabilization of the cameras. This configuration still contains the dampening plate for showing passive dampening effects. However with the motors locked, the cameras will not remain nadir which will skew images taken in flight. The third configuration. "Gimbal Locked and Dampening Plate Removed" removes the dampening plate and keeps the motors locked. This configuration emulates the most simple camera payload attachment directly onto the UAV.

As a control, an COTS gimbal was used under the same configuration set up. This COTS gimbal is based off the LD Storm Eye Brushless Gimbal Full Carbon Kit[17] as seen in Fig. 10 and outfitted with the same gimbal board and similar quality gimbal motors.
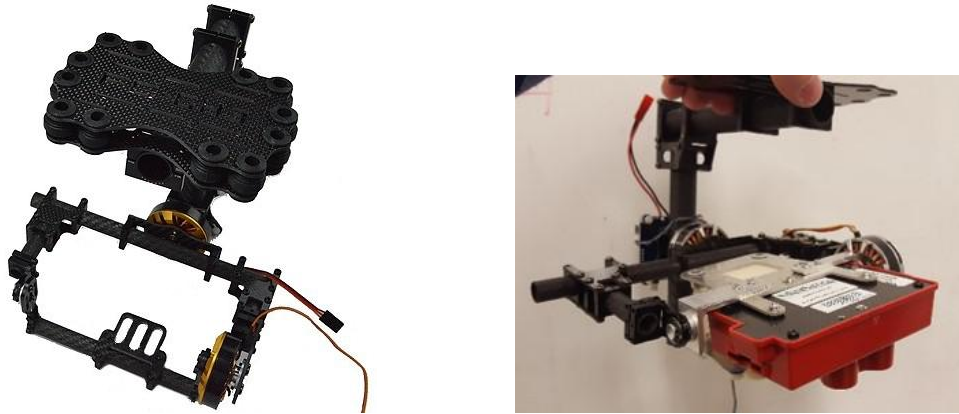
Fig. 10. LD Storm Eye Brushless Gimbal Full Carbon Kit shown on the left and COTS Gimbal outfitted with MAPSS Fixture Plate, FLIR Plate, and camera payloads on the right. While the RedEdge is clearly seen, the an FVPR model is located behind the RE near the center of the fixture plate of the COTS Gimbal.

The flight test was initially planned to be entirely autonomous, however for safety a remote pilot manually operated the test vehicle. While the remote pilot maintains line of sight with the S1000+, a Ground Control Station (GCS) operator monitors and relays in-flight altitude information to the remote pilot. Using this information, the remote pilot can maintain a rough altitude and respond swiftly to any flight changes while testing.

B.   Modulation Transfer Function (MTF)

Testing the RedEdge and FVPR image quality was done through taking images with the sensors while airborne and calculating the MTF curves of the footage. The MTF score, in this case, defines the resolution of contrast that the cameras can resolve.[24] The main function of the testing will determine how blurry an image is by looking at the MTF score of a crisp, high contrast slanted line during operation.[25] This modern slanted edge analysis is performed as an ISO 12233 standard to gauge the effectiveness of camera lenses.[26]

The process of calculating the MTF of a camera is normally done in a very controlled environment with leveled equipment, high contrast test objects, and specific lighting. While this was the optimal configuration for testing MAPSS as well, the expenses that came with a controlled testing stage and flying a drone in the same testing environment proved to be beyond the scope of this project. The relative score between images was used instead of the direct MTF values. Normal MTF testing requires MTF "test articles" to be placed in the center of the image and at the four corners, allowing for the lens' field of view and edge distortion to be characterized. This type of testing was attempted with some of the first flights of MAPSS by using white foam board with black paper adhered to the center with small aluminum bars in the center of the back paper. These MTF test articles were around 609mm by 457mm for the white foamboard and 215.9mm by 279.4mm for the black paper. The flights these articles were used in flew around 6.096m in the air and the corner test articles were 4.57m apart in the width of the image frame and 3.048m apart in the height of the image frame. An image from the flight is shown in Fig. 11. The black on white provided the visual contrast the RedEdge needs for MTF calculation while the cold, reflective aluminum and hot black paper provided the thermal contrast required for the FVPR, but requires further image processing. Since the FVPR is radiometrically calibrated, the sensor is capable of showing the absolute temperature of an object and temperatures within a specific range of $\pm 5°C$ for a reading between -25°C and 135°C and $\pm 20°C$ for a reading between -40°C and 550°C.[10] The test articles could not provide a large enough temperature

American Institute of Aeronautics and Astronautics

difference for Raw data taken from the FVPR. By processing raw data through ImageJ optimizing contrast, a visual contrast similar to the RedEdge can be seen in Fig. 11.
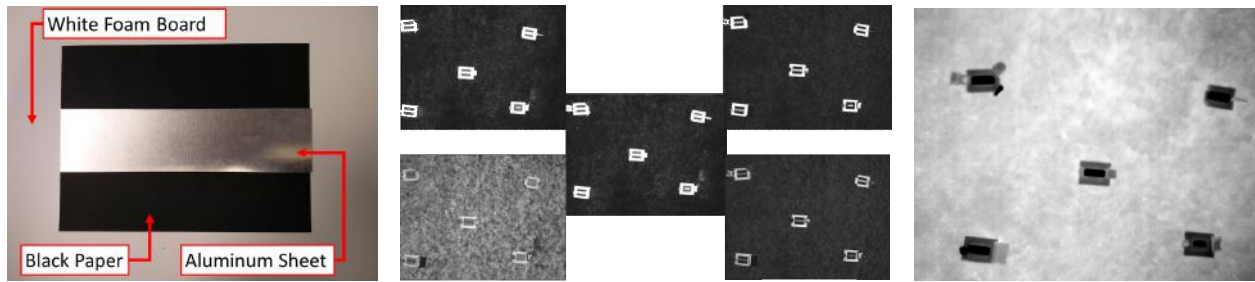
Fig. 11. The left image shows components of the small test MTF article. The center and right images shows in-flight images of the smaller MTF articles using the RedEdge and FVPR respectively. The center image shows the resulting images captured from each of the RedEdge channels; Blue, green, red, red edge, near-infrared. These images are then post-processed by MicaSense to produce maps seen in Fig. 2.

However, with the determination that a relative comparison of images could be used, a larger MTF test article was constructed. This new MTF article was made much larger due to the flight heights increasing to match a more reasonable flight altitude of 15.24m. While this is still much lower than most RedEdge flights, this height was flyable with the multirotor used for testing and allowed for a larger MTF test article without setup time and materials getting excessively large. The larger MTF test article moved away from conventional square test articles in favor of a rectangular shape allowing for longer edges to be analyzed. The white foamboard from before was replaced with a 6.096m by 3.048m black 6mil plastic. A white fabric previously used as a canopy for flight testing was cut into several 1.524m by 3.048m strips. These strips were laid out on the black plastic and went the full 6.096m length. With such a large black area the aluminum was given its own section along side the white canvas. Two separate lengths of 177.8mm aluminum flashing were stacked and adhered to the black plastic for the required thermal gradient. An example image from the test can be found in Fig. 12. Still image post-processing was utilized for the FVPR raw images to create false-color images optimized for contrast. The actual MTF analysis is taken from the larger MTF article and will be presented later in this paper.
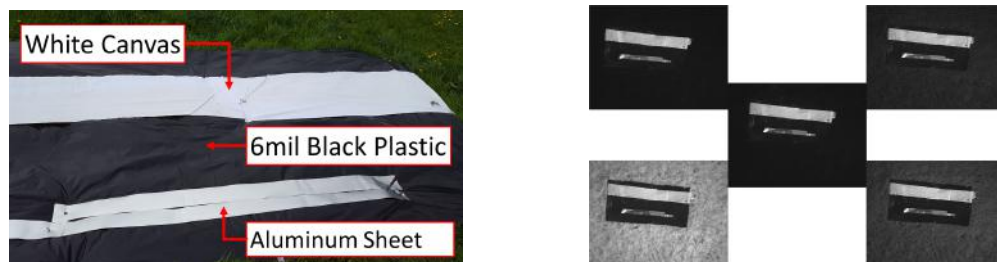
Fig. 12.   Images of the larger MTF test article offering longer edges to sample data from. The left image shows the larger MTF article consisting of a white canvas strip(located on upper half) and thin aluminum sheet (located on the bottom half) overlaying a black plastic background. The right image shows the in-flight images taken by the RedEdge. An example of in-flight image taken from the FVPR can be seen in Fig. 7.

C.   Vibration Analysis

To capture quality images, the gimbal needed to effectively deal with vibrations that can roughly be partitioned in two main categories, albiet with some overlap. The first category is lower frequency, large vibrations and angle changes. These are caused by the UAV maneuvering for the desired flight path and correcting for large gusts of wind. The large oscillations primarily have the negative effect of disrupting the nadir orientation of the cameras. The second category is smaller amplitude, high frequency vibrations, which are caused by the rotors of the UAV. These vibrations can affect the nadir orientation, but the main negative effect is the high frequency shaking of the cameras blurs the images, particularly in the FVPR, which has a rolling shutter.

American Institute of Aeronautics and Astronautics

The low frequency oscillations were controlled by brushless gimbal motors and the control board. The IMU provides feedback to a PID controller, which stabilizes the gimbal in pitch and roll. Analyzing these oscillations was initially done by viewing previous flight vibration data from the Pixhawk controller on the UAV. This gave a good initial idea of the expected disturbances, but it could not account for the highly variable wind forces that would act on the gimbal itself. Since wind gusts could come at any speed and any angle, wind tunnel testing was ruled out as insufficient and unreliable. The main method for verifying the active stabilization system would be making sure that images have the target in frame and not rotated and using an on-board vibration sensor to verify the nadir orientation.

IV.   Results

From the six flight tests, the MTF and vibration results from the RedEdge and FVPR were compared. The MTF analysis focused on the MTF Curves and MTF50 Score while the Vibration focused on the Vibration Amplitude in the Z direction and Fourier Transformed results. The MTF50 Score is a criteria for image sharpness as the spatial frequency located at an MTF of 0.5 indicates a general image quality for the overall MTF Curve.[26]

A.   MTF Results

1.   RedEdge Footage

Images were captured while hovering over the MTF article at 15.24m as a basis for in-flight vibration. Fig. 13, contains the MTF curves of the respective gimbals and their configurations.
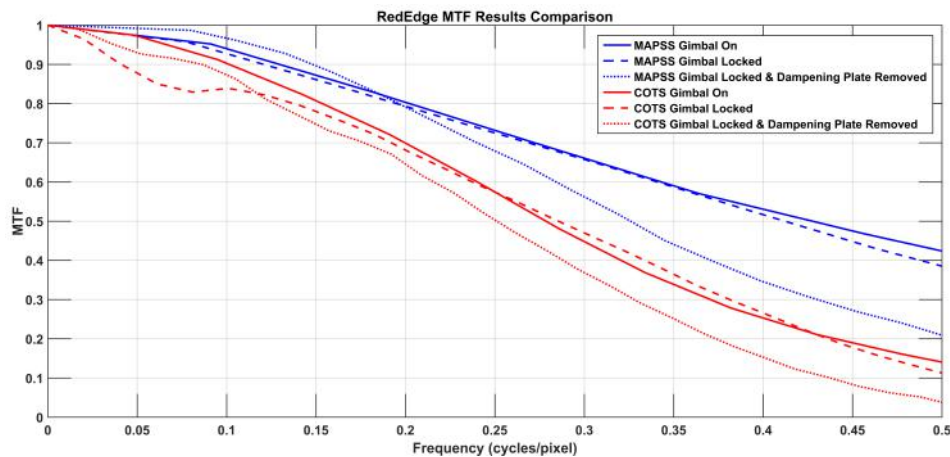
Fig. 13.   Overlay of RedEdge MTF data showing MAPSS higher resolution capabilities compared with the COTS Gimbal over all configurations. The MTF50 score for the Gimbal On and Gimbal Locked configurations are closer than expected for both MAPSS and the COTS Gimbal. However, the expected deterioration of the Gimbal Locked and Dampening Plate Removed Configuration results in worse results as expected.

From these curves, the MTF50 scores were used as an average quantification of resolution capabilities as seen in Table 3.

Table 3.   RedEdge MTF Analysis: MTF50 Score

Gimbal	Gimbal On	Gimbal Locked	Gimbal Locked and Dampening Plate Removed
COTS	0.2785	0.2855	0.2511
MAPSS	0.4275	0.4121	0.3258

In terms of the quality of images taken, MAPSS performed better overall when compared with the COTS Gimbal. In general the MTF curves decline as the spatial frequency increases and MTF decreases. However

American Institute of Aeronautics and Astronautics

from the 0 to 0.2 cycles per pixel frequency, the MTF curves perform not quite as expected. The COTS Gimbal Locked configuration degrades sharply then continues the expected smooth downward curve. The MAPSS Gimbal Locked and Dampening Plate Removed configuration degrades slowly, outperforming the other MAPSS configurations, then returns to its expected results. Continuing from 0.2 cycles per pixel the MTF curves perform as expected with Gimbal Locked and Dampening Plate Removed configuration performing the worst. The Gimbal On and Gimbal Locked configurations roughly supported similar performance. The COTS Gimbal Locked configuration performed better than its Gimbal On configuration within the 0.25 to 0.4 cycles per second range. While for MAPSS, the Gimbal On configuration performed better overall compared to its Gimbal Locked configuration. These results support that MAPSS can provide a significant increase in resolution of the images taken. However the FVPR with a rolling shutter may provide different results.

2. FLIR Vue Pro R Footage

The same process was performed with the FVPR footage to create Table 4 and combining datasets to create Fig. 14.
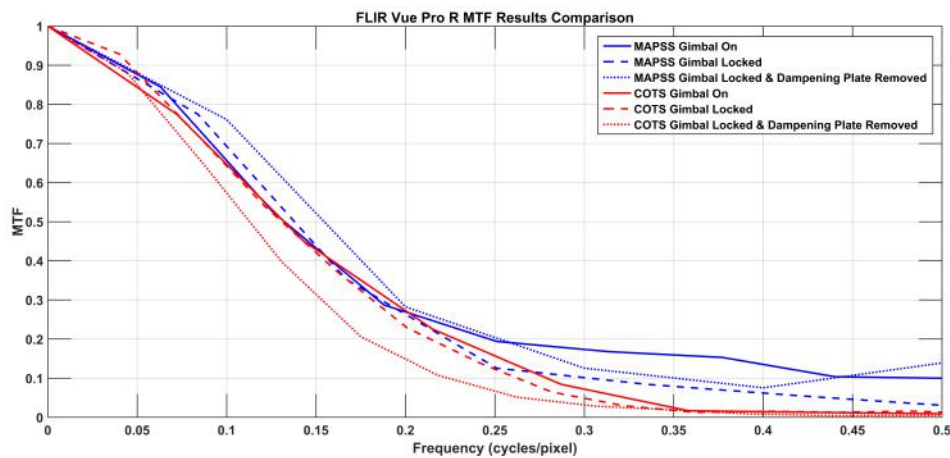

Fig. 14. Overlay of FVPR MTF data showing MAPSS higher resolution capabilities compared with the COTS Gimbal over all configurations. Compared to the RedEdge MTF Results, image quality differences between MAPSS and the COTS Gimbal are less prominent, but shows marginal increase in quality for MAPSS.

Table 4. FVPR MTF analysis: MTF50 score.

Gimbal	Gimbal On	Gimbal Locked	Gimbal Locked and Dampening Plate Removed
COTS	0.1322	0.1309	0.1129
MAPSS	0.1323	0.1379	0.1545

In general the MTF curves of the FVPR corresponds to the MTF curves of the RedEdge. In Fig. 14, the same overall results of MAPSS performing better than the COTS gimbal is shown. However there are significant differences within each configuration.

The COTS MTF curves perform as expected within all configurations with Gimbal On and Gimbal Locked out performing Gimbal Locked and Dampening Plate Removed. Similarly to the RE MTF curves, the Gimbal On and Gimbal Locked configurations perform similarly then at higher spatial frequencies the Gimbal On outperforms.

The MAPSS FVPR MTF curves perform similarly to the MAPSS RedEdge MTF curves the same relationship between the Gimbal On and Gimbal Locked configurations is apparent. Even the Gimbal Locked and Dampening Plate Removed configuration follows the same superior performance of the other configurations at the 0 to 0.2 cycles per pixel range.
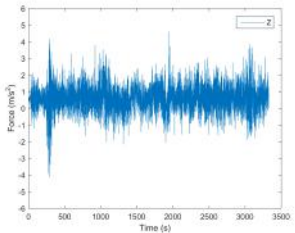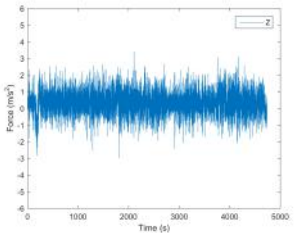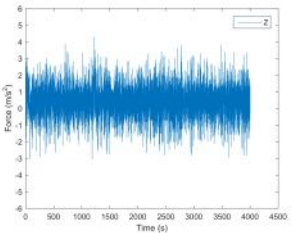
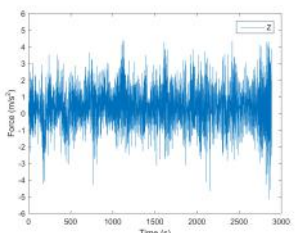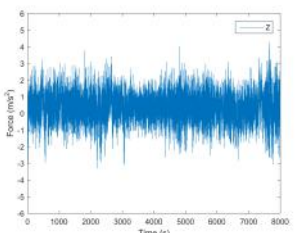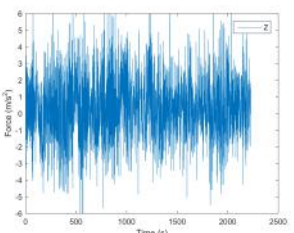American Institute of Aeronautics and Astronautics

B.   Vibration Results

Focusing on the vibrations on the fixture plate level in the Z axis while hovering offers insights into in-flight vibrations directly affecting the cameras. Compared to the X or Y axis vibrations, the majority of the in-flight vibration is expressed in the Z axis due to the propeller motors causing to counteracting gravity in a hover.

With larger vibration amplification, vibration data in the Z axis is easier to analyze and differentiate from noise.

For ease of analyzing the Z axis vibrations, a Fourier transform was performed on the flight test data. While noisy, the Fourier transform shows what frequencies within the 0 to 35 Hz range affected the fixture plate.

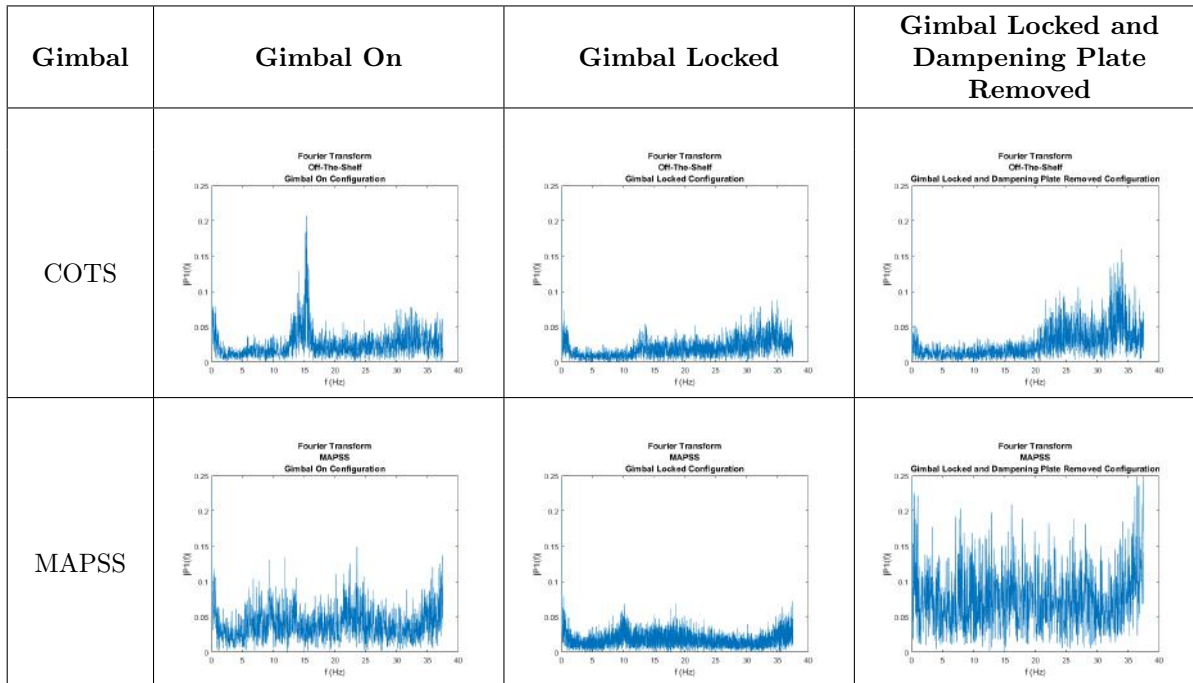Table 5. In-flight vibration in the Z axis.

Gimbal	Gimbal On	Gimbal Locked	Gimbal Locked and Dampening Plate Removed
COTS	$0.589\ m/s^2$ (std dev: 0.89)	$0.3449\ m/s^2$ (std dev: 0.80)	$0.4431 m/s^2$ (std dev 1.08)
MAPSS	$0.3564\ m/s^2$ (std dev: 1.23)	$0.3736\ m/s^2$ (std dev: 0.93)	$0.3928 m/s^2$ (std dev: 2.07)

From Table 5, a trend of the standard deviations of the six configurations can be seen. Higher amplitude vibrations occurred most with the "Gimbal Locked and Dampening Plate Removed" configuration followed by the "Gimbal On" configuration. Overall, MAPSS had higher standard deviation vibrations than the COTS gimbal.

Taking the Fourier transform leads to similar observations as seen in Table 6 in addition to any resonant frequencies within the gimbal configurations.

While noisy, some general trends are apparent within the data. Most notably, the COTS "Gimbal On" configuration contains a sharp peak at roughly 14.8 to 15.4 Hz. This peak is also somewhat noticeable in the "Locked" configuration. The MAPSS "Gimbal On" configuration contains increases at 6 to 14 Hz and 20 to 26 Hz. However these general increases are not seen in the "Locked" configuration. The MAPSS "Locked" configuration is similar to the COTS "Locked" configuration as both data sets contain a much smaller peak when compared to their respective "Gimbal On" configurations. The COTS "Gimbal Locked and Dampening Plate Removed" configuration was susceptible to higher frequency vibrations with a peak around 33.9 Hz. The same configuration on MAPSS contained mostly noise from the full 0 to 35 Hz spectrum.

American Institute of Aeronautics and Astronautics

Table 6. Fourier transform of in-flight vibration.

Gimbal	Gimbal On	Gimbal Locked	Gimbal Locked and Dampening Plate Removed
COTS			
MAPSS			

While the vibration data supports the usefulness for a dampening plate within a gimbal structure, the vibration results imply that the "Gimbal On" configurations allowed for more vibrations to permeate through the gimbal to the fixture plate level. This can be seen as the "Gimbal On" configuration allows for the gimbal motors to rotate from signals from the gimbal controller. With the "Locked" configuration, the gimbal motors are fixed and unable to rotate as freely. These results did not prevent the "Gimbal On" configuration from having the better RedEdge MTF score in Table 3. The FVPR MTF scores in Table 4 indicate that the "Gimbal On" and "Gimbal Off" scores were still very close even with the larger vibration differences.

C. Results Summary

The MTF comparisons of the COTS gimbal and MAPSS shows that the MAPSS takes higher quality images. RedEdge with higher resolution provided clearer data than the FVPR. MTF curves using both cameras show marginal differences between the "Gimbal On" and "Gimbal Locked" configurations.

In terms of vibration, the "Gimbal Locked" configurations dampened vibrations more effectively than the "Gimbal On" or "Gimbal Locked with Dampening Plate Removed" configuration. The difference between the "Gimbal On" configuration and the "Locked" configuration comes down to vibrations occurring while the gimbal motors are free to rotate. This issue could be mitigated by raising the center of gravity to be inline in all three directions with the gimbal motors, using more powerful gimbal motors, or changing the controller to have a faster response to higher frequency vibrations.

For image quality during a hover, MTF analysis and vibrations at the fixture plate level is conclusive for "Gimbal Locked" configurations. For "Gimbal On" configurations, gimbal motors and the gimbal motor controller must be sufficiently responsive to be able to negate vibrations from the gimbal motors.

Future image quality analysis while moving must be made with a UAV capable of autonomous flight to capture uniform footage. With manual flight, maintaining a uniform movement pattern 15.24m in the air while sufficiently capturing the MTF article was difficult to coordinate. Any hesitation from the person manipulating the controls may show up in the footage while moving.

D. Error Analysis

The MTF analysis in-flight is not as precise as the MTF analysis performed on the ground. With a grounded setup, controlled distances, and controlled light sources, more consistent MTF results is expected. Reproducing this experiment in-flight requires more consistency. Given more time, flight testing methodology would

American Institute of Aeronautics and Astronautics

need to be revised to include further testing under a control environment with stricter testing methodology and include more robust vibration data gathering.

A control environment such as an indoor flight test could be used to mitigate environmental factors such as lighting, temperature, and wind. Lighting in particular was potentially very different from one test to another, due to cloud coverage and time of day. Capturing images with the RedEdge at sunset gives different results than capturing at noon due to the way light travels through the atmosphere. The temperature gradient between the black plastic and aluminum may grow and shrink as the day passes, however as long as the highest and lowest temperature objects in the image are the black plastic and aluminum the results should not change substantially given post-processing. Removing wind as a factor creates reproducible results, but in-flight tests would still be required for a viable product.

In addition to the control environment, a stricter testing methodology would allow for reproducible results. A UAV following a strict path would account for any human errors from a remote pilot. The large MTF article would need to be revised to have precise straight edges to sample from and be able to provide the FVPR a larger temperature contrast to eliminate the need of image post processing. With these improvements, the images taken from multiple flights would be more identical. With these changes the MTF curves would become more precise than current methods.

Vibration analysis performed in this project was limited to gathering low frequency vibrations in specifically the Z axis. Gathering higher frequency vibrations or a larger range of frequencies offers a larger scale to compare more vibration differences. Vibrations in the X and Y directions can affect image quality not only by causing translations of the cameras, but also by rotation, since the center of gravity is positioned slightly below the axis of rotation, these inertial forces impart a moment to the payload plate.

In addition, gathering euler angle data while in-flight may offer clearer vibration and image quality correlation. Any noise in euler angle results would provide insights to how vibrations are causing MAPSS to clearly go off nadir skewing image results.

Tests were conducted on the ground to ensure nadir orientation of the gimbal while attached to the S1000+, but the nadir results while airborne could only be verified through video recordings of the system in flight. Attempts were made to ensure nadir orientation in the photos taken by the cameras through adding vertical structures that could have their areas compared to in data reduction, but this data ended up going uncollected in the field. Future flight tests planned on implementing this metric into the data collection procedure either through euler angle data or other means.

V.   Conclusions and Further Research

The gimbal described within this paper took several iterations and several dozen improvements to incrementally improve on the previous attempt. Further design modifications to reduce weight and further flight testing is required to perfect this iteration. The primary goal of this work is to provide MicaSense customers a gimbal option for their sensing needs. MAPSS, as a whole is intended to improve precision agriculture and provide farmers the ability to improve their data gathering processes. Essentially, the goal is to help growers take better pictures of their crops.

While the MTF data supports that MAPSS improves picture quality while hovering, repeatable experimentation under realistic agricultural photography scenarios and clearer criteria and correlation is needed. Gathering specific nadir orientation data and comparing with X and Y translation vibration would be preferential to proving MAPSS effectiveness. However, the MTF testing and analysis performed in this paper offers a useful method for quantifying sharpness from images taken from cameras mounted on a UAV.

Though more fixes must be made before MAPSS becomes a viable product, the main goal of the Senior Capstone Program, educating students through a rigorous team project incorporating industry standards was a success. With MicaSense's guidance, the students learned about transferring college education into real-life engineering scenarios, current manufacturing practices, and adapting to the needs of a time-sensitive engineering project. The students also gained valuable experience coordinating project vision and action within the team and industry partners.

In order to expand this project, more testing is required to ensure functionality for a wider range of usage scenarios and gathering more data. In the future MAPSS could be used for multiple UAV platforms ranging from multicopters to fixed-wing aircraft with modular camera payloads similar to existing research in precision agriculture.[27]

Acknowledgments

This research was supported by MicaSense Inc., the Autonomous Flight Systems Laboratory (AFSL), and the Aeronautics and Astronautics (AA) department of the University of Washington. We specifically thank Gabriel Torres and MicaSense for allowing us the opportunity to work on this project. We also thank the AA department Capstone coordination instructors, Professor Tony Waas and Professor Anshu Narang-Siddarth, and teaching assistants, Alexander Summers and Brian Leege. Finally, special thanks to AA research staff, Eliot George and Fiona Spencer, AA Financial Staff, Nancy-Lou Polk and Steve Pearson, and AFSL members, Hannah Rotta, Tadej Kosel, Zachary Williams, and Connor Kafka.

References

[1] Lum, C. W., Vagners, J., and Rysdyk, R. T., "Search Algorithm for Teams of Heterogeneous Agents with Coverage Guarantees," *AIAA Journal of Aerospace Computing, Information, and Communication*, Vol. 7, January 2010, pp. 1–31.

[2] Lum, C. W., Summers, A., Carpenter, B., Rodriguez, A., and Dunbabin, M., "Automatic Wildfire Detection and Simulation Using Optical Information from Unmanned Aerial Systems," *Proceedings of the 2015 SAE Aerotec Conference*, Seattle, WA, September 2015.

[3] Lum, C. W., Vagners, J., Vavrina, M., and Vian, J., "Formation Flight of Swarms of Autonomous Vehicles in Obstructed Environments Using Vector Field Navigation," *Proceedings of the 2012 International Conference on Unmanned Aircraft Systems*, Philadelphia, PA, June 2012.

[4] Lum, C. W., Mackenzie, M., Shaw-Feather, C., Luker, E., and Dunbabin, M., "Multispectral Imaging and Elevation Mapping from an Unmanned Aerial System for Precision Agriculture Applications," *Proceedings of the 13th International Conference on Precision Agriculture*, St. Louis, MO, August 2016.

[5] Livne, E. and Nelson, C. P., "From Blank Slate to Flight Ready New Small Research UAVs in Twenty Weeks-Undergraduate Airplane Design at the University of Washington," *Proceedings of the AIAA Aerospace Sciences Meeting (ASM)*, 2012.

[6] Livne, E., Valasek, J., Starkey, R., and Strganac, T., "Integrated Research/Education University Aircraft Design Program Development," Final report, University of Washington, Seattle, WA, 2017.

[7] "MicaSense Website," https://www.micasense.com/, Accessed November 24, 2017.

[8] "MicaSense RedEdge Data Sheet," MicaSense https://static1.squarespace.com/static/579a34a98419c24fcccb6be1/t/57b10db7197aeaae0ce68fcf/1471221177246/MicaSense_RedEdge_Datasheet_03.pdf, Accessed Feb 16, 2017.

[9] "MicaSense RedEdge Main Image," MicaSense https://www.micasense.com/rededge/, Accessed Feb 16, 2017.

[10] "FLIR Vue Pro R Main Image," FLIR http://www.flir.com/suas/vuepror, Accessed Feb 16, 2017.

[11] Rouse, J., Haas, R., Scheel, J., and Deering, D., "Monitoring Vegetation Systems in the Great Plains with ERTS," *Proceedings of the 3rd Earth Resource Technology Satellite (ERTS) Symposium*, Vol. 1, 1974, pp. 48–62.

[12] "MicaSense RedEdge Sample Data," MicaSense https://www.micasense.com/red-edge-sample-data, Accessed Feb 16, 2017.

[13] "Mini Power HUB w/ BEC 5V and 12V Datasheet," Matek Systems http://www.mateksys.com/downloads/HUB5V12V_Manual_V3.pdf, Accessed May 01,2017.

[14] "FVPR Datasheet," http://www.flir.com/uploadedFiles/sUAS/Products/Vue-Pro-R/FLIR-VUE-Pro-R-Datasheet-EN.pdf, Accessed Feb 16, 2017.

[15] "Fastenal Technical Reference Guide," https://www.fastenal.com/content/documents/FastenalTechnicalReferenceGuide.pdf, Accessed Feb 16, 2017.

[16] "Micro Plastics Mechanical Test Data," Micro Plastics Inc https://secure.microplastics.com/mechanicaldata.aspx, Accessed April 05, 2017.

[17] "LD Storm Eye Brushless Gimbal Full Carbon Kit," https://hobbyking.com/en_us/ld-storm-eye-brushless-gimbal-full-carbon-kit-dslr.html, Accessed Feb 20, 2017.

[18] Arduino, "MPU-6050 Accelerometer and Gyro," https://playground.arduino.cc/Main/MPU-6050, 2017, Accessed Feb 25, 2017.

[19] Rowberg, J., "I2cdevlib," https://github.com/jrowberg/i2cdevlib/tree/master/Arduino/MPU6050.

[20] "Spreading Wings S1000+," DJI https://www.dji.com/spreading-wings-s1000-plus, Accessed Nov 16, 2017.

[21] Federal Aviation Administration, "Fact Sheet - Small Unmanned Aircraft Regulations (Part 107)," June 2016.

[22] Lum, C. W., Larson, R. S., Handley, W., Lui, S., and Caratao, Z., "Flight Testing an ADS-B Equipped sUAS in GPS-Denied Environments," *Proceedings of the AIAA Flight Testing Conference*, Denver, CO, June 2017.

[23] Lum, C. W., Vagners, J., Jang, J. S., and Vian, J., "Partitioned Searching and Deconfliction: Analysis and Flight Tests," *Proceedings of the 2010 American Control Conference*, Baltimore, MD, June 2010.

[24] Burns, P., "Slanted-Edge MTF for Digital Camera and Scanner Analysis," Eastman Kodak Company http://www.losburns.com/imaging/pbpubs/26pics2000burns.pdf, Accessed March 03, 2017.

[25] Kurtsev, O., "Basic steps in calculating the MTF (SFR), and comparing it with the open-source tools sfrmat3 and Mitre SFR 1.4," http://www.quickmtf.com/slantededge.html, 2011.

[26] Estribeau M., M. P., "Fast MTF measurement of CMOS imagers using ISO 12233 slanted-edge methodology," .

[27] Valasek, J., Lu, H. H., and Shi, Y., "Development and testing of a customized low-cost unmanned aircraft system based on multispectral and thermal sensing for precision agriculture applications," *2017 International Conference on Unmanned Aircraft Systems (ICUAS)*, June 2017, pp. 1208–1216.